ADVANCED MATERIALS TECHNOLOGIES
www.advmattechnol.de

Micropatternable Janus Paper as a Wearable Skin Patch for Sweat Collection and Analysis

*Yang Gao and Seokheun Choi**

Single-use paper-based wearable devices are receiving increasing attention as a novel platform for disposable, inexpensive, noninvasive, and real-time sweat monitoring. The bidirectional liquid transport nature of paper is the most critical barrier to effectively controlling sweat samples for reliable and accurate sweat analysis. Excessive or additionally released sweat significantly interferes with analysis when mixed with old sweat. Moreover, bio-receptors pre-loaded in the sensing areas can backflow and move to another sensing region generating a cross-talk issue. This work enables effective sweat sampling and delivery in paper by facilitating unidirectional sweat transport from the skin to the sensing reservoir. The design and fabrication of a single-layered paper membrane to achieve Janus-type properties, which only allow moisture to flow in one direction is introduced. When the hydrophobic side of the Janus paper is placed on the skin, sweat is unidirectionally self-pumped from the hydrophobic side to the hydrophilic sensing areas, but not the reverse. The fabrication takes two steps including easy automatic and scalable printing of hydrophobic micropatterns on paper and simple heating of the printed paper for the wax penetration. Quantitative colorimetric assessment of pH, chloride, sodium, and glucose in sweat is simultaneously performed without cross-talk between the sensing regions.

1. Introduction

Noninvasive monitoring of sweat composition creates innovative and convenient opportunities for routine diagnostics with real-time insights into the status of the human body.[1,2] Sweat contains a rich variety of biochemical biomarkers, including electrolytes, metabolites, proteins, and hormones, that hold clinical relevance.[3–5] Skin-interfaced wearable biosensors have offered a range of modalities to analyze those biomarkers with capabilities in capturing, storing, and delivering sweat.[6–9] The ability of wearable sweat biosensors to continuously perform the functions for an extended period has become an intensively sought-after feature to acquire detailed diagnostic information.[10–12] To this end, the devices developed to date are confronted by a multitude of challenges that require changes to permit intimate and conformal skin contact with long-term user acceptance and sustainable energy harvesting integration for continuous operation without user intervention.[11,13–15]

Many wearable biosensors are typically designed for disposable single-use applications.[16–18] The devices can provide athletes with simple management guidance of electrolyte and water balance during physical activity.[19,20] Those rapid measurements of sweat constituents are particularly attractive in the context of point-of-care diagnostics that can provide immediately actionable healthcare information.[16,21–23] Those single-use wearables circumvent all the challenges and problems for the development of long-term wearable platforms such as lack of conformability, mechanical mismatch, power shortage, insufficient sweat quantities, and skin irritation.[10,11] Because the single-use devices run for special short-term missions and sufficient sweat is available through physical exercise, user compliance, local sweat simulation, and other technical requirements for prolonged monitoring with wearables are not major impediments. That allows short-term and single-use wearable applications to be much more commercially successful.[24,25] Moreover, surveys show that more than 30% of users stopped wearing the devices within 6 months because of discomfort, loss of motivation, frequent charging requirements, routine malfunctions, and sensing inaccuracies.[10,11] These statistics indicate a potential for a market increase even in one-time or short-term wearable biosensors parallel to long-term high-fidelity counterparts.

Recently, paper has been extensively explored as a promising substrate material for single-use wearable applications because of its intrinsic breathability, biocompatibility, and flexibility.[26] Although paper lacks stretchability and may impose fatigue and discomfort for wearers, its limited applications for short-term periods, and its miniaturizable and integrable characteristics mitigate those concerns. Rather, paper's easy liquid handling capability through capillary action with its rich surface chemistry offers the transformative potential of generating important functions for sweat collection and analysis simply and cost-effectively.[26–29]

Y. Gao, S. Choi
Bioelectronics & Microsystems Laboratory
Department of Electrical & Computer Engineering
State University of New York at Binghamton
Binghamton, NY 13902, USA
E-mail: sechoi@binghamton.edu
S. Choi
Center for Research in Advanced Sensing Technologies & Environmental Sustainability
State University of New York at Binghamton
Binghamton, NY 13902, USA

The ORCID identification number(s) for the author(s) of this article can be found under https://doi.org/10.1002/admt.202300396

DOI: 10.1002/admt.202300396

Moreover, the compatibility of paper to mature printing processes and its novel functionalization techniques with various materials enable simple and cost-effective engineering possibilities, setting up the paper-based techniques for wearable applications.[30] Meanwhile, the biodegradability and eco-friendliness of paper have attracted much attention for single-use disposable applications, reducing the dramatic increase in electronic waste.[18,31,32] Many paper-based wearable sensors have been developed for noninvasive sweat sensing and analytics with the capability of passive sweat sampling.[26,27,33,34] In particular, colorimetry has been recently unveiled as the most suitable sensing technique for single-use, wearable paper-based platforms, offering rapid, simple, and cost-effective point-of-care diagnostics by the naked eye.[26,34]

Despite these superiorities and proof-of-concept demonstrations of paper as a wearable sensor, our ability to harness the potential of paper lags from a lack of effective sweat collection and transportation for reliable and precise sweat analysis. When single-use diagnostic testing is usually performed during physical exercise, the body continuously secretes a large amount of sweat, and conventional papers with isotropic wettability are quickly filled for rapid analysis. However, excessive or additionally released sweat interferes with accurate analysis of available biomarkers by being continuously mixed with old sweat.[35,36] Pre-inoculated reagents for multiplex colorimetric detection can flow in the reverse direction and move to other sensing regions, inducing cross-talk between biosensors. Most traditional papers that are used for wearable applications have bidirectional wicking behavior.[37] Moreover, this property can slow the sweat sampling when moisture is absorbed from a humid environment in the opposite direction.[38] When the paper is fully saturated, the nonabsorbed excessive sweat remains between the skin and paper, weakening the mechanical strength of the paper and developing a wet, sticky microenvironment.[35,36] Even worse, the accumulated sweat may promote the breeding of bacteria, causing potential infections with a peculiar smell.[39] Therefore, conventional paper with symmetric wettability is very limited in sweat sampling for accurate analysis and excessive sweat removal from the skin to address the aforementioned major problems.

Previously, effective sweat sampling and delivery have been facilitated by directional sweat transfer through a Janus membrane possessing different wettability on opposing sides abruptly shifting from hydrophobic to hydrophilic.[35,36] When the hydrophobic side of the Janus membrane contacts the skin and the hydrophilic region including the biosensors faces air, then the sweat can be unidirectionally self-pumped from the hydrophobic side to the hydrophilic sensing areas, but not the reverse (**Figure 1**a). Driven by the Laplace pressure, the directional transport removes excess sweat away from the skin and keeps it dry (Figure 1b). A specific amount of sweat can be confined in the sensing region for accurate and reliable analysis without interference from excessive sweat or a reverse flow from other sensing areas. Unfortunately, the most studied forms of Janus membranes have been mainly Janus fabrics or Janus textiles.[35,36,40] Commercial Janus fabrics are available with sportswear and outerwear for effective moisture and thermal management.[39,41,42] Even, various Janus fabrics and Janus polymer membranes have been explored for sweat sampling and analysis,[35,36,40,43] wound healing,[44–46] and facial masking.[47] However, in the literature, reported work on Janus-type paper was quite limited[37] or unavailable for wearable applications. Even the latest advances in Janus-type paper membranes are limited to selective oil–water separation[48,49] and require very complicated, time-consuming steps which are not compatible with batch fabrication and microelectromechanical systems techniques for miniaturized wearable platforms.[37,48,50] No other studies have proposed a Janus-type paper that can be readily microfabricated for wearable, skin-interfaced sweat sensors.

In this work, we report, *for the first time*, a microfabricable, skin-mountable Janus-type paper that can facilitate unidirectional sweat transport while effectively delivering the sweat to the sensing areas and improving the sensing accuracy (Figure 1). Moreover, our wearable Janus paper removes excess sweat from the skin and maintains a comfortable epidemic microenvironment (Figure 1a,b). This work demonstrates a simple approach to fabricating a flexible, wearable Janus substrate with a single sheet of paper by double-sided wax printing and heat-treatment for asymmetric wettability integration across the paper thickness (Figure 1c). Multiplexed colorimetric assays built on the Janus paper allow reliable and distinct identifications of multiple analytes without any cross-talk (Figure 1d). After use, the Janus paper was simply disposed of by incineration (Figure 1e).

2. Results and Discussion

2.1. Fabrication and Unidirectional Water Transport Capability of Janus Paper

Fabrication of single-layered Janus paper involves two simple steps: easy automatic printing of hydrophobic micropatterns on paper with a commercial solid wax printer (Xerox ColorQube 8570DN) and rapid and simple heating of the printed paper in an oven for the wax penetration. This wax printing and melting technique has been widely used for paper-based electronics and paper-based microfluidics because it is rapid, inexpensive, and batch fabricable.[51,52] Above all, the printed wax patterns can be formed with vertical and horizontal dimensions of less than several hundred micrometers by controlling the temperature and the time in the oven.[53] Recent double-sided wax-printing allowed more versatility and flexibility in design and fabrication as the printed wax can penetrate from both directions.[54] Moreover, because hydrophobic patterning with wax does not require any further chemical or toxic reagents and the wax itself is nontoxic,[42] our entire process is completely environmentally friendly. However, much of this revolutionary technique has been limited only to the development of paper-based devices and has not been used to create a Janus membrane. Simple and easy formation of hydrophobic and hydrophilic regions within a single piece of paper will open up a new avenue to prepare monolayered Janus substrates having different wetting properties in a cost-effective and scalable way.

To provide insights into the fabricability and wetting properties of Janus paper, we prepared a miniature Janus substrate by printing wax on both sides of Whatman Chromatography Paper (3MM; 180 μm thick) and melting it at 150 °C for 40 s (Figure S1, Supporting Information). It takes only 3 min from printing to the end of the heating process. The wax was printed and heated to form an inverted U-shaped pattern (Figure S1, Sup-

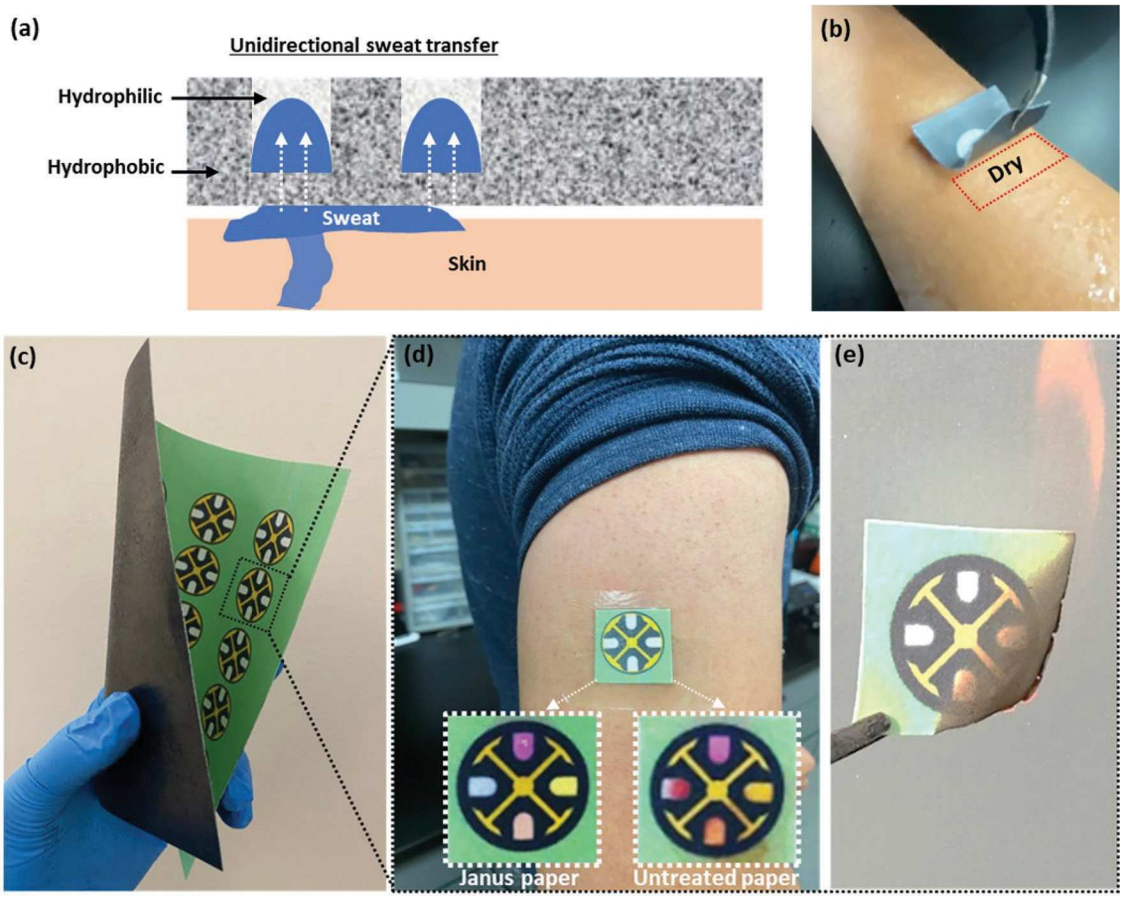

Figure 1. Conceptual images of the proposed Janus paper and its application for sweat analysis. a) Directional sweat transport process. b) Janus paper faced on sweaty skin. c) Photoimage of the Janus paper biosensors batch-fabricated in a single sheet of paper. d) Photoimages of the Janus biosensors applied on skin and its distinct color changes while cross-talk occurs with untreated paper biosensors. e) Disposal of the Janus paper biosensors by incineration.

porting Information). The horizontal stroke of the inverted U penetrated the paper to about 90 μm. The pattern's hydrophobic boundaries were completed when the melted wax met on the peripheries. The dimensional chamber volume was designed to be 0.16 μL, but the actual volume for liquid storage will be much less considering all the cellulose fibers located within the chamber. To visually characterize unidirectional liquid transport through the Janus region, we deposited a 5 μL red droplet on the hydrophilic chamber which has an actual volume of 0.07 μL. When the droplet was put on the hydrophobic side (the contact angle: 105°), it was directly pumped through the hydrophobic layer and wetted the hydrophilic layer (Figure S2a, Supporting Information). When the hydrostatic pressure (F_H; downward) and the Laplace pressure (F_L; downward) overcome the hydrophobic pressure (F_p; upward) on the hydrophobic side, the water droplet will penetrate the hydrophobic layer.[44,55] Because hydrostatic pressure (F_H) is the fluidic pressure caused by gravity, the mass of the droplet will be the critical variable. The Laplace pressure (F_L) can be generated when the water droplet contacts a porous material and is defined by the following equation[55,56]

$$F_L = \frac{2\gamma_L}{R} = \frac{-p\gamma_L(\cos\theta)}{S} \quad (1)$$

where γ_L is the surface tension of the droplet and R is the radius of the droplet on the hydrophobic material surface. p is the perimeter of the substrate pores, θ is the contact angle of the droplet on the surface, and S is the area of the pore. When the droplet passes through the hydrophobic layer and contacts the hydrophilic region below, there will be two strong driving forces added, the capillary force (F_C) of the hydrophilic layer and the surface tension (F_A) of the accumulated droplets there, achieving the unidirectional liquid transport from the hydrophobic to hydrophilic layer (Figure S2a, Supporting Information). On the other hand, the droplet dropped on the hydrophilic side (the contact angle: 27°) of Janus paper spread over the hydrophilic layer without penetrating the hydrophobic layer (Figure S2b, Supporting Information). The horizontal component of the capillary force and the surface tension cannot overcome the hydrophobic force in the vertical direction opposite to the water penetration. When the droplet is placed on a thick hydrophobic membrane with the wax through the entire paper thickness (the contact angle: 131°), it can never pass through the membrane because of the very strong hydrophobic force (Figure S2c, Supporting Information).

The droplets continued to be dropped on the hydrophobic side of Janus paper (**Figure 2**). The first droplet was enough to

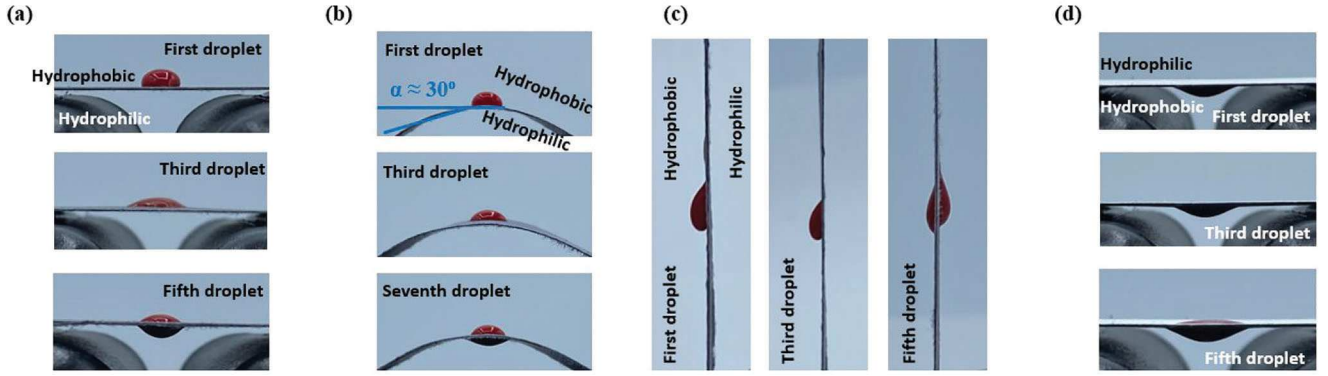

Figure 2. Snapshots of the water transport phenomenon with the increasing number of droplets through Janus paper when a) it was placed horizontally and the water was dropped on the hydrophobic side facing upward, b) it was curved and the water was dropped on the hydrophobic side, c) it was placed vertically and the water was applied to the hydrophobic side, and d) it was flipped (hydrophilic side facing upward) and the water was applied to the hydrophobic side facing down.

enable the directional water transfer through the hydrophobic layer and get the hydrophilic chamber wet below (Figure 2a). However, it did not exert sufficient downward pressure to accumulate beneath the paper as the miniature hydrophilic chamber was quickly filled decreasing its capillary force and surface tension. When the fifth droplet was added with the built-up hydrostatic pressure, water dripped from below. When the Janus paper was bent by 30°, more droplets were needed to drip (Figure 2b). The mechanical deformation may decrease the hydrostatic pressure on the curved hydrophobic layer and reduce the chamber volume with decreasing capillary force and surface tension. This unidirectional liquid transport capability of Janus paper also was demonstrated when the paper was placed vertically (Figure 2c) or the hydrophobic side faced down (Figure 2d). In particular, Figure 2d shows that the droplet can penetrate the hydrophobic layer even in the antigravity direction and the fifth droplet allowed some water accumulation above the hydrophilic surface, indicating that the force for unidirectional water transport can be strong enough and well controlled. However, with this miniature Janus membrane, the additional droplets against gravity do not generate enough force to continuously drive the unidirectional liquid transport through the membrane and form a large droplet from the hydrophilic surface.

The hydrophilic chamber dimension, the thickness of the hydrophobic layer, and the porosity of the hydrophobic layer will play a pivotal role in the unidirectional liquid transport of the proposed Janus paper. The size and volume of the hydrophilic chamber determine the capillary pressure and surface tension while the thinner hydrophobic layer reduces the hydrophobic pressure and the larger pore size in the hydrophobic layer increases the Laplace pressure, leading to better directional transport performance. Those three parameters are interrelated in a way that the penetration depth of the wax-based hydrophobic region will modulate the volume of the hydrophilic region within the single sheet of paper and the porosity of the hydrophobic part during the wax infiltration. To characterize the relationship between these three parameters and optimize the procedure for the best performance, we modified the fabrication steps so that the hydrophobic layer in the Janus membrane can be independently controlled from the hydrophobic boundaries (Figure S3, Supporting Information). Moreover, the diameter of the hydrophilic region was increased so that its dimensional volume reached 10.18 µL for more practical water storage. Changes in heating time determined the porosity and the thickness of the region bounded by the penetrated wax and the volume of the hydrophilic region below. Through scanning electron microscopy (SEM) characterization, we investigated the surface morphology and porosity changes of the bare paper sheet and the wax-printed paper sheets with increasing heating time at 150 °C (**Figure 3**a). When the wax was first printed and did not go through the heat treatment, the pores of the original bare paper were blocked. However, with increased wax heating time, the structure had more pores, demonstrating that the breathable and porous nature of the paper can be preserved even with the paper engineered to have a Janus membrane. At the same time, the wax penetrated further through the paper increasing the thickness of the hydrophobic layer while decreasing the volume of the hydrophilic region (Figure 3b). Heat treatment for more than 50 s allowed the wax to penetrate almost the entire thickness of the paper, leaving no room for the hydrophilic layer. The wetting properties were characterized according to heating time by dropping a droplet on each side of Janus paper (Figure 3c). Without heat treatment or with a 20 s heat treatment, the paper showed bidirectional liquid transport because of the very thin hydrophobic layer. With 30 and 40 s heat treatment, unidirectional liquid transport was observed, and the liquid required only about 15 s to pass through the Janus membrane. However, the red ink did not evenly spread out in 30 s. With the 50 s heating, the liquid requires more than 3 min to reach the hydrophilic side. Heat treatment for 60 s did not penetrate the liquid at all because hydrophobic layer became too thick. With a 40 s heating time at 150 °C, the porosity and the thickness of the wax and the hydrophilic layer dimension were optimized to provide the best performance in unidirectional water transport.

Moreover, in order to provide more insight of the composition of the Janus membrane, X-ray diffractometer (XRD) and scanning electron microscopy with energy dispersive X-ray spectrometer were performed (Figure S4, Supporting Information). XRD has confirmed that the chronography paper used was composed by cellulose Iβ.[57,58] The printed wax did not change the polymeric structure of the cellulose but only added

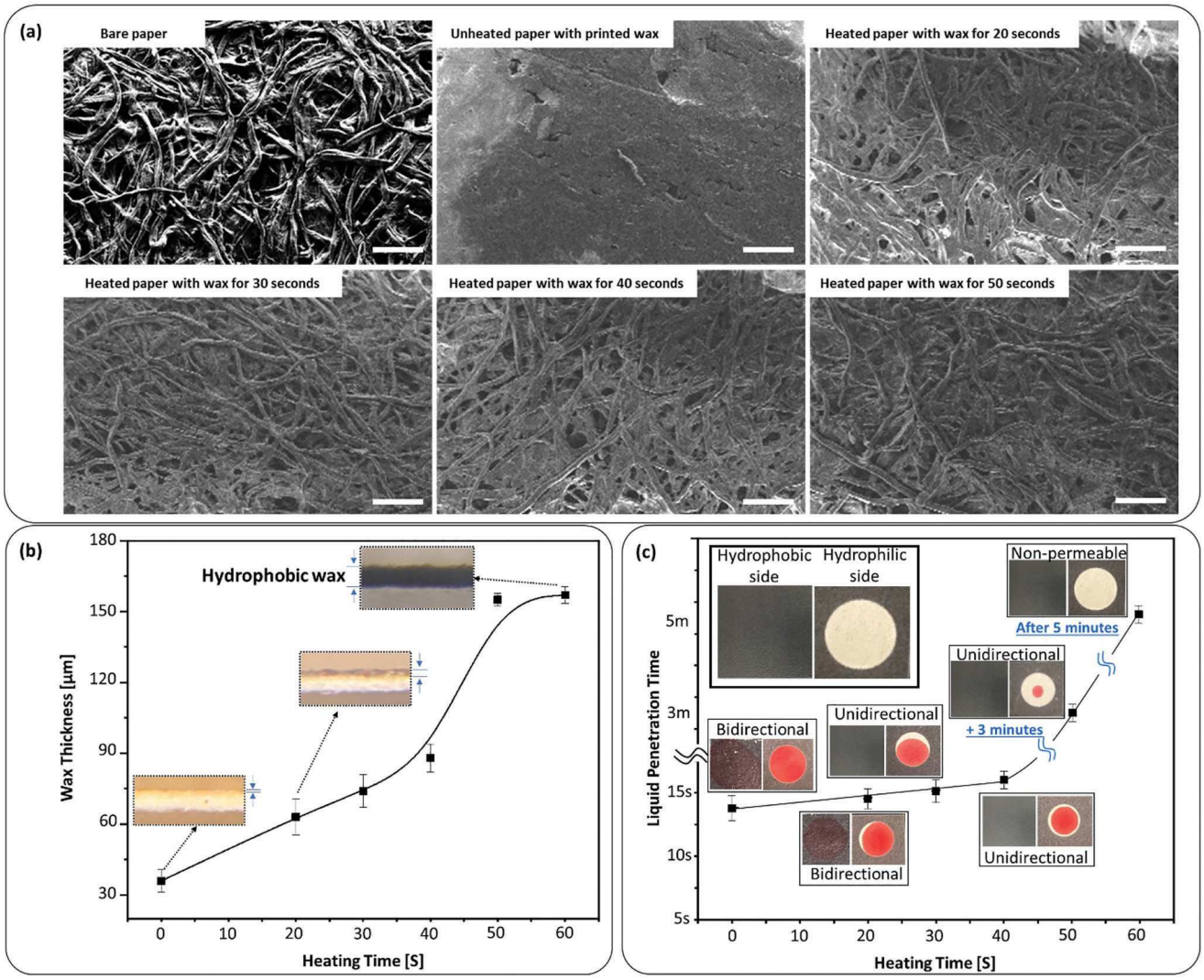

Figure 3. a) SEM images, b) wax thickness, and c) wetting properties and liquid penetration time with increasing wax heating time.

some more carbon, oxygen, and silicon elemental groups. These results indicated that the Janus paper can be highly safe and eco-friendly, providing a promising substrate for the fabrication of wearable devices.

2.2. Wearable and Disposable Janus Paper for Sweat Collection and Analysis

Prior to the tests, we first measured the contact angle of paper to real sweat as presented in Figure S5 in the Supporting Information. The author's sweat was collected after working out. As sweat is mainly water, the result was similar to that of Figure S2 in the Supporting Information, demonstrating that the Janus membrane can potentially achieve unidirectional transfer even with sweat. The unidirectional liquid transport capability of Janus paper shows great potential in effectively collecting sweat samples and reducing an undesired wet and sticky microenvironment. When the hydrophobic side of Janus paper was placed on the red-dyed ink, the paper stably floated on the ink and absorbed it until the hydrophilic chamber was completely filled (**Figure 4**a). Because the strong hydrophobic pressure at the interface between the paper and ink repels water and the capillary pressure and the surface tension in the hydrophilic area considerably decrease as the ink permeates the area, no more ink will pass through the membrane and accumulate once the hydrophilic area is fully saturated. Even when we relocated the red-ink-saturated Janus paper onto the blue-dyed ink, no additional ink infiltration was observed. Moreover, the red ink in the hydrophilic region did not get out and contaminate the blue ink. When the paper was not designed to have hydrophobic–hydrophilic asymmetry but to include hydrophilic region only, the red-ink-soaked area continuously wicked the blue ink (Figure 4b). Rather, the red ink flowed in the reverse direction and polluted the blue ink (Figure S6, Supporting Information). The entirely hydrophobic paper did not absorb any red or blue ink at all (Figure 4c). This soak-and-retain property of Janus paper allows the effective collection and precise analysis of a sweat sample. Absorbed sweat will not be mixed

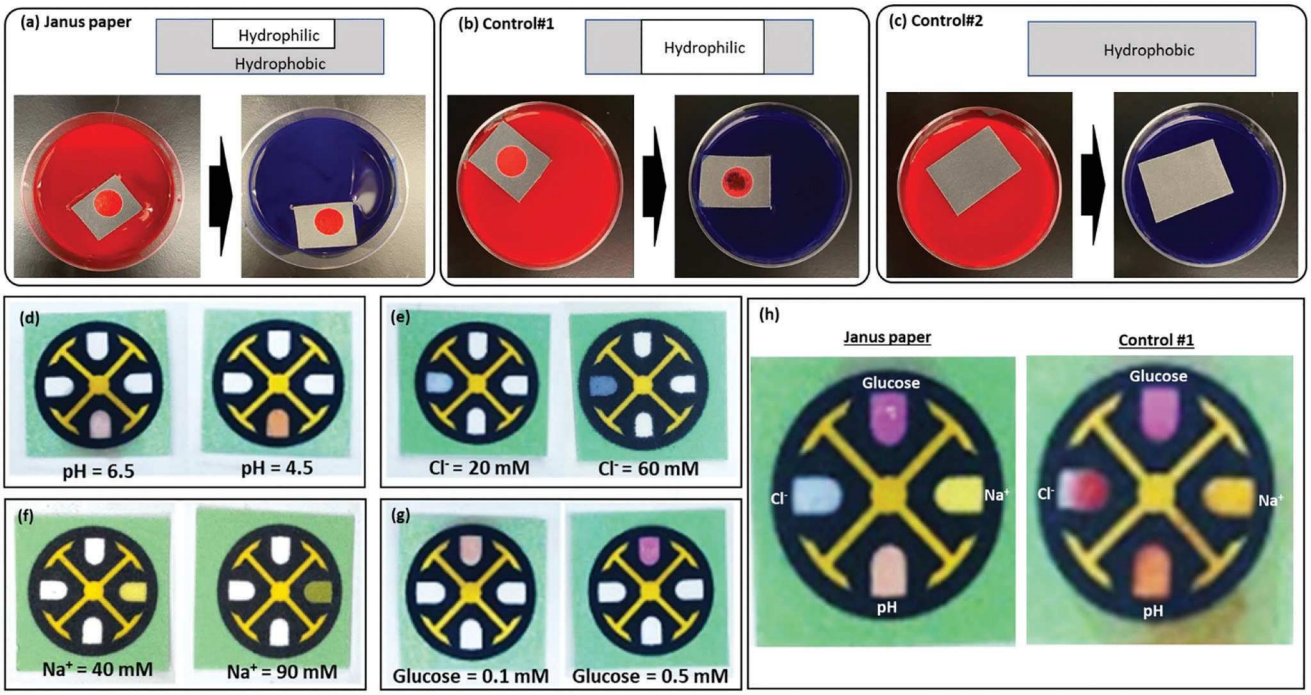

Figure 4. Wetting properties of a) Janus paper, b) hydrophilic paper as control #1, and c) hydrophobic paper as control #2. Each paper was placed on the red ink for 15 s and then replaced on the blue ink. Colorimetric assays for individual assessment of d) pH, e) chloride (Cl^-), f) sodium (Na^+), and g) glucose and h) simultaneous analysis of all four biomarkers in sweat.

with excessive or additionally released sweat and any chemical compounds pre-loaded in the hydrophilic area will never come out of the Janus paper. As shown in Figure 4d–h, the Janus paper was designed to include four pre-loaded reagents for colorimetric analysis which enabled quantitative assessment of pH, chloride (Cl^-), sodium (Na^+), and glucose in sweat.[6,59,60] The colorimetric sensors and the hydrophobic–hydrophilic asymmetric structure were simply batch-fabricated by double-sided wax-printing and subsequential heat treatment (Figure S7, Supporting Information). pH is normally considered an indicator of thermal regulation and dehydration. The pH indicator yields colorimetric responses over the epidermally relevant change of the sweat pH from a normal range of 6.5 to an acidic 4.5 (Figure 4d). Chloride and sodium are the most important ions because chloride helps diagnose cystic fibrosis and sodium shows altered electrolyte levels.[57,59] The presence of chloride induces a change in color from transparent to blue (Figure 4e). Sodium ions in the sample produce a color change from yellow to green (Figure 4f). Glucose concentration as a direct diabetes biomarker can be monitored while immobilized glucose oxidase produces hydrogen peroxide (H_2O_2), generating a purple color along with the increase of glucose concentration (Figure 4g).[57] Through unidirectional sweat transport through the Janus paper, each sensing chamber provided a specific, quantitative chemical analysis of a different physiological issue. When the Janus paper with all four colorimetric assay reagents was placed on the surface of the sweat, the sweat was effectively sampled by each sensor and quantitatively assessed for each biomarker (Figure 4h). The Janus paper did not permit crosstalk between individual sensors while all sensors in the control only with the hydrophilic region were contaminated by each other's reagent, hampering efficient sweat analysis. For the control, a pre-loaded reagent was flowed in the reverse direction and moved to another sensor with a different reagent.

Moreover, sweat sensors integrated into the Janus paper demonstrated better sensitivity and performance during the electrochemical reactions between the reagents and the sweat. Three electrodes (i.e., working, counter, and reference electrodes) were screen-printed on the hydrophilic side of Janus paper and the control without the asymmetric wetting contrast, which were both placed on potassium chloride (KCl) electrolyte for cyclic voltametric measurements (Figures S8, Supporting Information and **Figure 5**a,b). According to the different KCl concentrations, the Janus paper showed superior sensitivity and better electrochemical activity than the control (Figure 5a). The electrochemical responses occurred only with the electrolyte contained in the hydrophilic area of Janus paper while the control was continuously interfered by the liquid replacement. The Janus paper shows a more linear square root of the scan rate than the control, indicating that the Janus paper provides a more diffusion-controlled and reversible environment (Figure 5b).

The mechanical performance of the Janus paper was tested. The fabricated device was repeatedly folded and stretched until the wax coating was fully broken. A tolerance of more than 30 cycles was achieved, indicating an outstanding mechanical stability for wearable applications (Figure S9, Supporting Information). In addition to the performance enhancement, the unidirectional sweat transport of Janus paper can effectively remove excessive sweat from the skin and create a dry and comfortable microenvironment, avoiding potential bacterial infections and a peculiar smell. When the blue-ink-covered glass was faced with

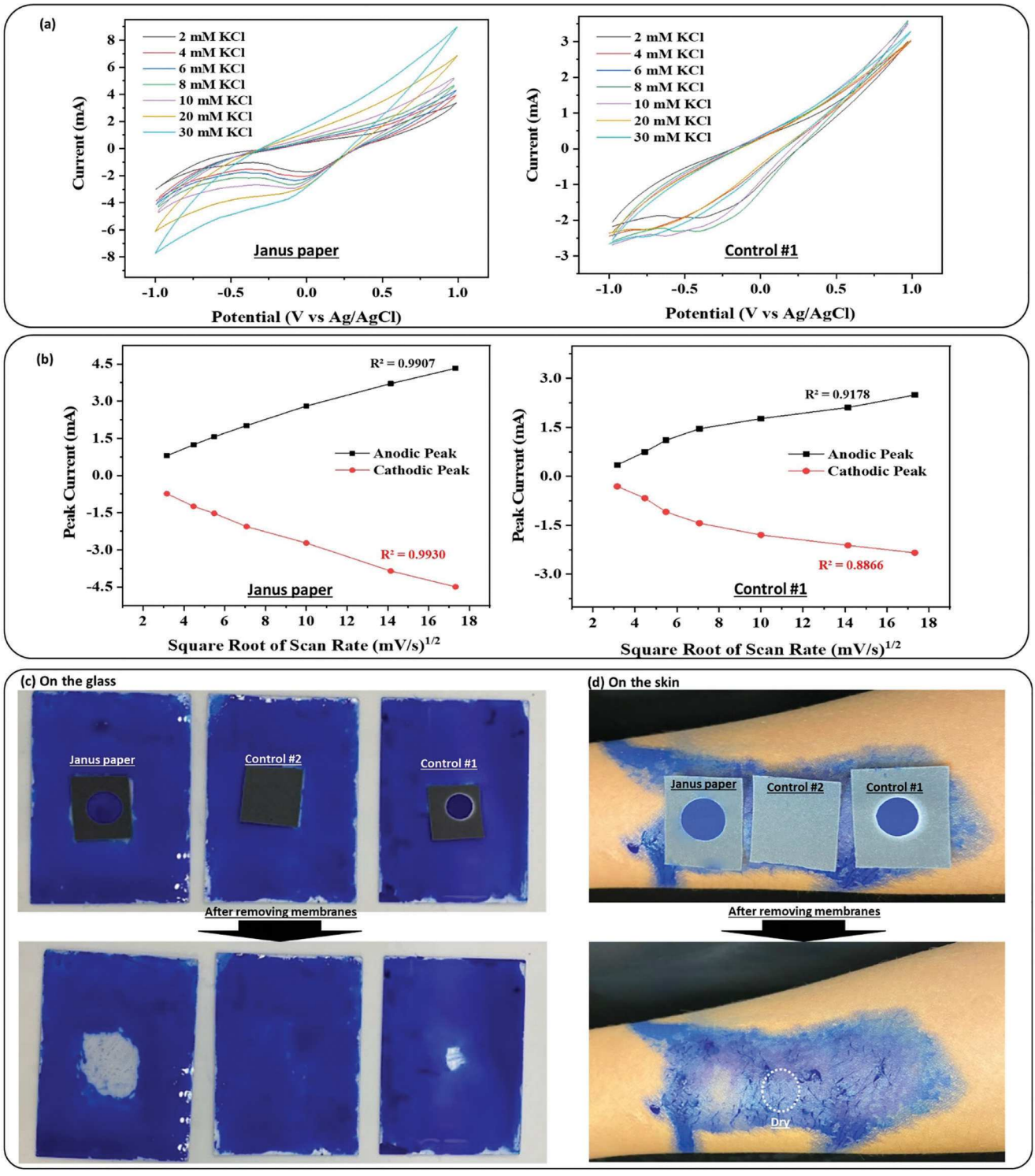

Figure 5. Electrochemical characteristics of three-electrode systems constructed on Janus paper and hydrophilic paper (control #1). a) CV profiles at the scan rate of 500 mV s^{-1} in different KCl concentrations. b) Plots of anodic and cathodic peak currents versus square root of scan rates in 10 × 10^{-3} M KCl. Absorbance and dryness testing of Janus paper on c) blue-ink covered glass and d) author's arm. It produced a larger dry area than did the hydrophilic paper (control #1) and the hydrophobic paper (control #2).

the hydrophobic side of Janus paper, a larger dry area was observed than with the two controls: the entirely hydrophobic paper and the paper with a middle hydrophilic area surrounded by hydrophobic boundaries (Figure 5c). Even on uneven and nonuniform skin, the blue ink was effectively removed by the Janus paper, creating a dry surface while either control could keep the skin dry (Figure 5d). The Janus paper-based sensing system was very flexible and wearable, making conformal contact with the skin through 3 M Tegaderm medical transparent tape (Figure 1d). The paper can be easily disposed of by incineration after use. Figure S10 in the Supporting Information shows the Janus paper-based device was completely decomposed in 20 s. Disposability is a critical requirement for one-time use applications especially when it comes to sweat sensors to remove the risk of biowaste infection.

3. Conclusion

This work presents a facile, microfabricable, and scalable method to create a hydrophobic–hydrophilic Janus membrane on paper for wearable and disposable detection of sweat analytes. The paper-based membrane with asymmetric wetting characteristics was simply created by double-sided printing through a commercial wax printer and subsequent heat treatment in an oven for less than a minute. The technique is eco-friendly because wax is nontoxic and environmentally safe. By regulating the wax penetration and porosity, unidirectional sweat transport was realized in a single-layered paper substrate. Once the sweat passed through a hydrophobic layer and filled a hydrophilic chamber, no more excessive sweat was absorbed and no reverse flow occurred, achieving the sensitive detection of multiple biomarkers in sweat without cross-talk. Moreover, the hydrophobic layer facing the skin repelled the excessive sweat and the unidirectional sweat transport facilitated the absorbance of sweat underneath, leading to the effective removal of sweat and producing a dry surface. Our smart Janus paper was able to pump off sweat to targeted sensing sites, improving sweat sampling in paper-based devices, and holding great promise for wearable, disposable, and noninvasive sweat analysis.

4. Experimental Section

Materials: Whatman Chromatography Paper (3MM), potassium chloride (KCl), sodium chloride (NaCl), D-Glucose, potassium ferricyanide ($K_3[Fe(SCN)_6]$), and mercury thiocyanate ($Hg(SCN)_2$) were purchased from Sigma-Aldrich. Blue and red inks were purchased from Cosco Industries, Inc. Phosphoric acid (H_3PO_4) was purchased from Consolidated Chemical & Solvents LLC. pH indicator solution, chloride assay kit, sodium assay kit, and glucose assay kit were all purchased from Abcam PLC. Graphite ink (E3449) and silver/silver-chloride (Ag/AgCl, E2414) ink were acquired from Ercon Inc.

Preparation of Janus Paper: All device wax patterns were defined on paper by printing the hydrophobic wax with a commercial printer (Xerox Phaser, ColorQube 8570) and partially penetrating the paper by heat treatment at 150° for different duration. The patterns were designed using AutoCAD.

Water Contact Angles: Water contact angles (WCAs) of the Janus paper, hydrophilic paper (Control #1), and superhydrophobic paper (Control #2) were measured by a contact angle measuring instrument (Theta Lite system, Biolin scientific). A droplet of distilled water was deposited on the surface of each paper. The shape of the individual droplet was recorded and analyzed using ImageJ software. At least five measurements were taken for each sample and then the average WCAs were calculated.

Electrochemical Characterizations: CV measurements were performed using a potentiostat (Squidstat Plus, Admiral Instruments) in KCl solutions. The three-electrode system was designed with AutoCAD. Graphite ink served as the working and counter electrodes. Ag/AgCl ink was screen-printed as the reference electrode.

Colorimetric Assays: Colorimetric analysis reagents were spotted in their respective test zones on Janus paper. A 5 µL volume of a universal pH indicator solution served as a chromogen for pH detection. A chloride detection reagent (3 µL; chloride assay kit) was titrated with 0.1 wt% $Hg(SCN)_2$ until a clear appearance provided the functional component of the chloride assay reservoir. For the detection of sodium ions, β-Galactosidase (β-Gal) was first diluted 1:200 by adding 1 µL of β-Gal to 199 µL of 10×10^{-3} M dithiothreitol in sodium assay buffer. The obtained solution was then incubated at 37 °C for 10 min while being protected from light. After incubation, 100 µL sodium developer and 1 wt% $K_3[Fe(SCN)_4]$ were added. Preparation of the glucose detection assay involved dissolving glucose oxidase, horseradish peroxidase, and an OxiRed indicator into a sodium citrate buffer solution. A small volume (2 µL) of this cocktail was introduced into the glucose detection reservoir. Real human sweat samples were taken from the authors, but in vitro experiments were conducted. All of these assays were allowed to dry before use. Individual testing solutions (pH = 4.5 and 6.5; $Cl^- = 20 \times 10^{-3}$ and 60×10^{-3} M; $Na^+ = 40 \times 10^{-3}$ and 90×10^{-3} M; glucose = 0.1×10^{-3} and 0.5×10^{-3} M) were prepared accordingly.

Supporting Information

Supporting Information is available from the Wiley Online Library or from the author.

Acknowledgements

This work was supported by the National Science Foundation (ECCS #1920979 and ECCS #2020486). An informed written consent from all human participants was obtained prior to the research.

Conflict of Interest

The authors declare no conflict of interest.

Data Availability Statement

The data that support the findings of this study are available from the corresponding author upon reasonable request.

Keywords

directional liquid transport, hydrophilic/hydrophobic interfaces, Janus papers, sweat sampling, sweat sensing, wearable electronics

Received: March 13, 2023
Revised: May 3, 2023
Published online:

[1] J. Heikenfeld, A. Jajack, B. Feldman, S. W. Granger, S. Gaitonde, G. Begtrup, B. A. Katchman, *Nat. Biotechnol.* **2019**, *37*, 407.

[2] R. Ghaffari, D. S. Yang, J. Kim, A. Mansour, J. A. Wright Jr., J. B. Model, D. E. Wright, J. A. Rogers, T. R. Ray, *ACS Sens.* **2021**, *6*, 2787.
[3] M. Bariya, H. Y. Y. Nyein, A. Javey, *Nat. Electron.* **2018**, *1*, 160.
[4] J. R. Sempionatto, J. A. Lasalde-Ramírez, K. Mahato, J. Wang, W. Gao, *Nat. Rev. Chem.* **2022**, *6*, 899.
[5] Z. Sonner, E. Wilder, J. Heikenfeld, G. Kasting, F. Beyette, D. Swaile, F. Sherman, J. Joyce, J. Hagen, N. Kelley-Loughnane, R. Naik, *Biomicrofluidics* **2015**, *9*, 031301.
[6] W. Gao, S. Emaminejad, H. Y. Y. Nyein, S. Challa, K. Chen, A. Peck, H. M. Fahad, H. Ota, H. Shiraki, D. Kiriya, D.-H. Lien, G. A. Brooks, R. W. Davis, A. Javey, *Nature* **2016**, *529*, 509.
[7] J. Heikenfeld, A. Jajack, J. Rogers, P. Gutruf, L. Tian, T. Pan, R. Li, M. Khine, J. Kim, J. Wang, J. Kim, *Lab Chip* **2018**, *18*, 217.
[8] J. Choi, R. Ghaffari, L. B. Baker, J. A. Rogers, *Sci. Adv.* **2018**, *4*, eaar3921.
[9] F. J. Zhao, M. Bonmarin, Z. C. Chen, M. Larson, D. Fay, D. Runnoe, J. Heikenfeld, *Lab Chip* **2020**, *20*, 168.
[10] S. Xu, J. Kim, J. R. Walter, R. Ghaffari, J. A. Rogers, *Sci. Transl. Med.* **2022**, *14*, eabn6036.
[11] T. Stuart, J. Hanna, P. Gutruf, *APL Bioeng.* **2022**, *6*, 021502.
[12] M. C. Brothers, M. DeBrosse, C. C. Grigsby, R. R. Naik, S. M. Hussain, J. Heikenfeld, S. S. Kim, *Acc. Chem. Res.* **2019**, *52*, 297.
[13] S. Wang, J. Y. Oh, J. Xu, H. Tran, Z. Bao, *Acc. Chem. Res.* **2018**, *51*, 1033.
[14] Y. Liu, M. Pharr, G. A. Salvatore, *ACS Nano* **2017**, *11*, 9614.
[15] T. Huynh, H. Haick, *Adv. Mater.* **2018**, *30*, 1802337.
[16] C. Dincer, R. Bruch, E. Costa-Rama, M. T. Fernandez-Abedul, A. Merkoçi, A. Manz, G. A. Urban, F. Güder, *Adv. Mater.* **2019**, *31*, 1806739.
[17] S. Liu, D. S. Yang, S. Wang, H. Luan, Y. Sekine, J. B. Model, A. J. Aranyosi, R. Ghaffari, J. A. Rogers, *EcoMat* **2023**, *5*, e12270.
[18] Y. Gao, M. Rezaie, S. Choi, *Nano Energy* **2022**, *104*, 107923.
[19] D. R. Seshadri, R. T. Li, J. E. Voos, J. R. Rowbottom, C. M. Alfes, C. A. Zorman, C. K. Drummond, *npj Digital Med.* **2019**, *2*, 72.
[20] B. Muniz-Pardos, S. Sutehall, K. Angeloudis, J. Shurlock, Y. P. Pitsiladis, *Front. Sports Act. Living* **2019**, *1*, 38.
[21] H. Lee, C. Song, Y. S. Hong, M. Kim, H. R. Cho, T. Kang, K. Shin, S. H. Choi, T. Hyeon, D. Kim, *Sci. Adv.* **2017**, *3*, e1601314.
[22] S. Mondal, N. Zehra, A. Choudhury, P. K. Iyer, *ACS Appl. Bio Mater.* **2021**, *4*, 47.
[23] S. Zhang, J. Zeng, C. Wang, L. Feng, Z. Song, W. Zhao, Q. Wang, C. Liu, *Front. Bioeng. Biotechnol.* **2021**, *9*, 774210.
[24] ReportLiner. Disposable Medical Device Sensor Market Research Report: Global Forecast to 2025, https://www.globenewswire.com/news-release/2021/01/22/2162900/0/en/Disposable-Medical-Device-Sensor-Market-Research-Report-by-Placement-of-Sensors-by-Product-by-Application-Global-Forecast-to-2025-Cumulative-Impact-of-COVID-19.html (accessed: January 2023).
[25] Allied Market Research. Wearable Patch Market by Product (Temperature Patch, Blood Glucose Patch, Blood Pressure Patch, Heart Rate Patch & ECG Patch, Skin Care Patch, and Others) and End Use (Healthcare and Fitness and Sports): Global Opportunity Analysis and Industry Forecast, 2020–2027, https://www.alliedmarketresearch.com/wearable-patch-market-A10358 (accessed: February 2023).
[26] Y. Xu, Q. Fei, M. Page, G. Zhao, Y. Ling, S. B. Stoll, Z. Yan, *iScience* **2021**, *24*, 102736.
[27] P. B. Deroco, D. Wachholz Junior, L. T. Kubota, *Electroanalysis* **2023**, *35*, 2200177.
[28] A. Vaquer, E. Baron, R. de la Rica, *ACS Sens.* **2022**, *7*, 488.
[29] T. Chu, J. Chu, B. Gao, B. He, *Analyst* **2020**, *145*, 5388.
[30] Y. Gao, S. Choi, *Adv. Mater. Technol.* **2018**, *3*, 1800118.
[31] T. Abbasiasl, F. Mirlou, E. Istif, H. C. Koydemir, L. Beker, *Sens. Diagn.* **2022**, *1*, 775.
[32] M. Mohammadifar, S. Choi, *Adv. Mater. Technol.* **2017**, *2*, 1700127.
[33] U. Mogera, H. Guo, M. Namkoong, M. S. Rahman, T. Nguyen, L. Tian, *Sci. Adv.* **2022**, *8*, eabn1736.
[34] Z. Yao, P. Coatsworth, X. Shi, J. Zhi, L. Hu, R. Yan, F. Guder, H. Yu, *Sens. Diagn.* **2022**, *1*, 312.
[35] X. He, S. Yang, Q. Pei, Y. Song, C. Liu, T. Xu, X. Zhang, *ACS Sens.* **2020**, *5*, 1548.
[36] Z. Peng, R. Liu, Z. Xu, H. Chi, Z. Wang, Y. Zhao, *Appl. Mater. Today* **2022**, *29*, 101623.
[37] M. Nau, N. Herzog, J. Schmidt, T. Meckel, A. Andrieu-Brunsen, M. Biesalski, *Adv. Mater. Interfaces* **2019**, *6*, 1900892.
[38] Y. Xia, C. Kan, *Coatings* **2022**, *12*, 301.
[39] J. Zhao, Z. Xu, S. Liu, T. Zhang, L. Huang, *Macromol. Mater. Eng.* **2021**, *306*, 2000578.
[40] X. He, C. Fan, T. Xu, X. Zhang, *Nano Lett.* **2021**, *21*, 8880.
[41] L. Lao, D. Shou, Y. S. Wu, J. T. Fan, *Sci. Adv.* **2020**, *6*, eaaz0013.
[42] B. Xu, Y. Ding, A. Li, *Adv. Mater. Interfaces* **2022**, *9*, 2200438.
[43] X. He, T. Xu, Z. Gu, W. Gao, L. Xu, T. Pan, X. Zhang, *Anal. Chem.* **2019**, *91*, 4296.
[44] J. Zhang, B. Liu, X. Liu, D. Wang, B. Dong, Y. Zhang, B. Xu, C. Chen, Z. Shen, *Macromol. Mater. Eng.* **2022**, *307*, 2200026.
[45] M. Song, Q. Zhao, X. Wang, C. Shi, X. Hu, J. Li, *Fibers Polym.* **2022**, *23*, 2511.
[46] L. Shi, X. Liu, W. Wang, L. Jiang, S. Wang, *Adv. Mater.* **2019**, *31*, 1804187.
[47] Y. Si, C. Guo, X. Xu, K. Zhang, R. Tan, K. Lau, J. Hu, *ACS Sustainable Chem. Eng.* **2022**, *10*, 7726.
[48] B. Xu, Y. Ding, *Adv. Mater. Interfaces* **2022**, *9*, 2200934.
[49] M. Zhang, Q. Yang, M. Gao, N. Zhou, J. Shi, W. Jiang, *J. Environ. Chem. Eng.* **2021**, *9*, 106016.
[50] C. K. Soz, S. Trosien, M. Biesalski, *ACS Appl. Mater. Interfaces* **3018**, *10*, 37478.
[51] M. M. Hamedi, A. Ainla, F. Guder, D. C. Christodouleas, M. Fernandez-Abedul, G. M. Whitesides, *Adv. Mater.* **2016**, *28*, 5054.
[52] M. Landers, A. Elhadad, M. Rezaie, S. Choi, *ACS Appl. Mater. Interfaces* **2022**, *14*, 45658.
[53] E. Carrilho, A. W. Martinez, G. M. Whitesides, *Anal. Chem.* **2009**, *81*, 7091.
[54] S. Jeong, S. Lee, C. Choi, J. Kim, C. Lee, *Lab Chip* **2015**, *15*, 1188.
[55] L. Yan, X. Yang, Y. Zhang, Y. Wu, Z. Cheng, S. B. Darling, L. Shao, *Mater. Today* **2021**, *51*, 626.
[56] R. Zhu, M. Liu, Y. Hou, L. Zhang, M. Li, D. Wang, D. Wang, S. Fu, *ACS Appl. Mater. Interfaces* **2020**, *12*, 50113.
[57] F. Needham, J. Reid, *Personal Communication*, **2009**.
[58] Y. Nishiyama, P. Langan, H. J. Chanzy, *J. Am. Chem. Soc.* **2002**, *124*, 9074.
[59] A. Koh, D. Kang, Y. Xue, S. Lee, R. M. Pielak, J. Kim, T. Hwang, S Min, A. Banks, P. Bastien, M. C. Manco, L. Wang, K. R. Ammann, K. I. Jang, P. Won, S. Han, R. Ghaffari, U. Paik, M. J. Slepian, G. Balooch, Y. Huang, J. A. Rogers, *Sci. Transl. Med.* **2016**, *8*, 366.
[60] S. Jadoon, S. Karim, M. R. Akram, A. K. Khan, M. A. Zia, A. R. Siddiqi, G. Murtaza, *Int. J. Anal. Chem.* **2015**, *2015*, 164974.